16

Secretory Vesicle Swelling by Atomic Force Microscopy

Sang-Joon Cho and Bhanu P. Jena

Summary

The swelling of secretory vesicles has been implicated in exocytosis, but the underlying mechanism of vesicle swelling remained unknown. Earlier studies from our laboratory demonstrated the association of the α-subunit of heterotrimeric GTP-binding protein $G_{\alpha i3}$ with zymogen granule membrane and implicated its involvement in vesicle swelling. Mas7, an active mastoparan analog known to stimulate Gi proteins, was found to stimulate the GTPase activity of isolated zymogen granules and cause swelling. Increase in vesicle size in the presence of GTP, NaF, and Mas7 were irreversible and found to be KCl sensitive. However, Ca^{2+} had no effect on zymogen granule size. Taken together, these results indicated that zymogen granules, the membrane-bound secretory vesicles in exocrine pancreas, swell in response to GTP mediated by a $G_{\alpha i3}$ protein. Subsequently, our studies demonstrated that the water channel aquaporin-1 (AQP1) is also present at the zymogen granule membrane and participates in rapid GTP-induced and $G_{\alpha i3}$-mediated vesicular water gating and swelling. Isolated zymogen granules exhibit low basal water permeability. However, exposure of granules to GTP results in a marked potentiation of water entry. Treatment of zymogen granules with the known water channel inhibitor Hg^{2+} is accompanied by a reversible loss in both the basal and GTP-stimulable water entry and vesicle swelling. Introduction of AQP1-specific antibody raised against the carboxy-terminal domain of AQP1 blocked GTP-stimulable swelling of vesicles. Our results demonstrate that AQP1 associated at the zymogen granule membrane is involved in basal GTP-induced and $G_{\alpha i3}$-mediated rapid gating of water into zymogen granules of the exocrine pancreas.

Key Words: Secretory vesicle; AFM; swelling.

1. Introduction

Secretory vesicle swelling is critical for exocytosis *(1–4)*; however, the underlying mechanism of vesicle swelling remains unknown. In mast cells, increase in secretory vesicle volume following stimulation of secretion had been suggested from electrophysiological measurements *(5)*. The requirement of osmotic force in the fusion of phospholipid vesicles with a membrane bilayer

From: *Methods in Molecular Biology, vol. 319: Cell Imaging Techniques: Methods and Protocols*
Edited by: D. J. Taatjes and B. T. Mossman © Humana Press Inc., Totowa, NJ

had also been demonstrated *(4,6,7)*. Isolated zymogen granules (ZGs), the membrane-bound secretory vesicles in exocrine pancreas and parotid glands, posses Cl^- and ATP-sensitive K^+ selective ion channels at the vesicle membrane, whose activities are implicated in vesicle swelling *(8–16)*. Additionally, secretion of ZG contents in permeabilized pancreatic acinar cells requires the presence of both K^+ and Cl^- ions *(2)*. In vitro ZG–pancreatic plasma membrane fusion assays demonstrate potentiation of fusion in the presence of GTP and NaF (*2,17*, unpublished observation). Heterotrimeric $G_{\alpha i3}$ protein has been implicated in the regulation of both K^+ and Cl^- ion channels in a number of tissues *(18–22)*. Analogous to the regulation of K^+ and Cl^- ion channels at the cell membrane, the regulation of K^+ and Cl^- ion channels at the ZG membrane by a $G_{\alpha i}$ protein was demonstrated *(17)*. Isolated ZGs from exocrine pancreas swell rapidly in response to GTP and NaF *(17)*. These studies suggest the involvement of rapid water entry into ZGs following exposure to GTP. As opposed to osmotic swelling, membrane-associated water channels called aquaporins have been implicated in rapid volume changes in cells *(23,24)* and intracellular vesicles *(25,26)*. Therefore, the likely mechanism of ZG swelling via possible water channels at the ZG membrane was explored *(27)*. Our study demonstrates the presence of aquaporin-1 (AQP1) in ZG membranes and its participation in $G_{\alpha i3}$-mediated and GTP-induced vesicle water entry and swelling *(27)*.

2. Materials and Methods

2.1. Cell Fractions

Rat pancreatic fractions were prepared and their purity determined as described elsewhere *(28–30)*. Salt and detergent treatment of isolated ZG membrane preparations were performed at 4°C for 30 min. Following treatment, supernatant and particulate fractions were separated by centrifugation of the reaction mixture at 4°C for 1 h at 200,000*g*.

2.2. Immunoblot Analysis

Immunoblot analysis was performed on pancreatic fractions prepared as described in **ref.** *26*. Protein in pancreatic fractions was estimated by the Bradford method *(31)*. Pancreatic fractions were boiled in Laemmli reducing sample preparation buffer *(32)* for 5 min. Equal loads of protein were resolved by 12.5% sodium dodecyl sulfate–polyacrylamide gel electrophoresis (SDS-PAGE), followed by electrotransfer to 0.2-μ*M* nitrocellulose sheets. The nitrocellulose was incubated for 1 h at room temperature in blocking buffer (5% nonfat milk in phosphate-buffered saline [PBS] containing 0.1% Triton X-100 and 0.02% NaN_3) and immunoblotted for 2 h at room temperature with either affinity-purified B-CHIP (AQP1) antibody raised against the holoprotein *(32)* (a gift from B. Baum and M.A. Knepper) or monoclonal vesicle-associated

membrane protein (VAMP) antibody recognizing VAMP1 and VAMP2 from StressGen Biotechnologies Corp. Both primary antibodies were used at a dilution of 1 : 1000 in blocking buffer. The immunoblotted nitrocellulose sheets were washed in PBS containing 0.1% Triton X-100 and 0.02% NaN_3 prior to incubation for 1 h at room temperature in horseradish peroxidase (HRP)-conjugated secondary antibody at a dilution of 1:2000 in blocking buffer. The immunoblots were washed in PBS containing 0.1% Triton X-100 and 0.02% NaN_3, processed for enhanced chemiluminescence and exposure to X-OMAT-AR film. The exposed films were then developed and photographed.

2.3. Immunoelectron Microscopy

Sections were prepared from rat pancreatic lobules embedded in unicryl and double immunogold labeling performed *(33)* using affinity-purified polyclonal rabbit anti-$G_{\alpha i3}$ and an antibody raised to the carboxy terminal of AQP1. Sequential labeling and visualization involved blocking steps and the use of 10 nm gold-conjugated anti-rabbit and 5 nm gold-conjugated goat antibody.

2.4. Atomic Force Microscopy

Isolated ZG suspensions in 125 μ*M* KCl–Mes buffer, pH 6.5, were plated on Cell-Tak-coated glass cover slips. Ten minutes after plating, the cover slips were placed in a fluid chamber and washed with the KCl–Mes buffer to remove unattached granules, prior to imaging the attached ZG in KCl–Mes buffer or water, in the presence or absence of various concentrations of GTP, 25 μ*M* $HgCl_2$, and 100 μ*M* β-mercaptoethanol. AQP1 antibody raised against the carboxy-terminus domain of AQP1 (Santa Cruz) was introduced into the ZG lumen by incubating the ZG at 4°C for 5 min in KCl–Mes buffer containing streptolysin-O (SLO) and the antibody or vehicle, followed by a 2-min incubation at 30°C and three washes in ice-cold 125 m*M* KCl–Mes buffer, pH 6.5. At 4°C, the SLO binds to the cholesterol molecule at the ZG membrane, making approx 14-nm holes at 30°C, which allow antibodies (approx 8 nm) to enter the ZG. Washing ZG with ice-cold 125 m*M* KCl–Mes buffer reseals the holes and removes ZG-associated SLO. Following incubation, the ZGs containing AQP1 antibody or the vehicle were washed and imaged in the presence of 40 μ*M* GTP. ZG imaging and dynamics were performed using the Nanoscope IIIa, an AFM from Digital Instruments (Santa Barbera, CA). ZGs were imaged both in the "contact" and "tapping" mode in fluid *(34,35)*. However, all images presented in this manuscript were obtained in the "tapping" mode in fluid, using silicon nitride tips with a spring constant of 0.06 N/m and an imaging force of less than 200 nN. Images were obtained at line frequencies of 2 Hz, with 512 lines per image, and constant image gains. Time-dependent (resolution in seconds) morphological changes in ZG were obtained using section analysis. Topographical

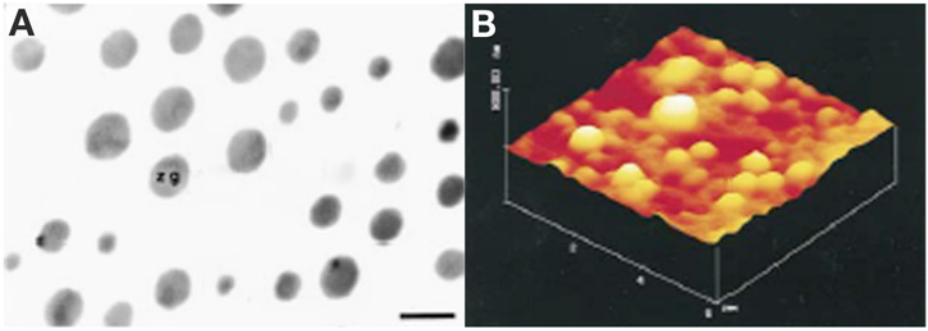

Fig. 1. Isolated ZGs ranging in size from 0.2 to 1.2 μ*M* obtained from rat pancreas as seen by electron microscopy and AFM. **(A)** An electron micrograph of the electron-dense ZGs. Note the purity of the ZG preparation. (bar = 1 μ*M*). **(B)** A three-dimensional AFM image of isolated ZGs adhering to a Cell-Tak-coated mica sheet. Note the size heterogeneity in the ZG population. (From **ref.** *17*.)

dimensions of ZG were analyzed using the software nanoscopeIIIa 4.43r8 supplied by Digital Instruments.

2.5. Measurement of Tritiated Water Entry

Isolated ZGs in 100 m*M* MES buffer, pH 6.5, containing 50,000 cpm of tritiated water were exposed to different stimulators, inhibitors, or their respective controls. The reaction mixture was incubated at room temperature for 30 min; ZGs were collected by centrifugation and tritiated water incorporation into them was estimated by liquid scintillation counting.

3. Results and Discussion

3.1. Purity and Size Heterogeneity of ZGs

The purity of ZGs was determined by imaging the isolated ZGs using a TEM (**Fig. 1A**). **Figure 1A** is an electron micrograph of the purified electron-dense ZGs with no detectable subcellular contaminants. When isolated ZGs plated on Cell-Tak-coated mica sheets were placed in 125 m*M* Mes buffer (pH 6.5) and imaged by the AFM, three-dimensional images were obtained (*see* **Fig. 1B**) that demonstrated a size heterogeneity in the ZG population. Measurements of ZG images obtained by AFM demonstrated that the diameter of ZGs range from 0.2 to 1.2 μ*M*.

3.2. Association of Gi3 With ZGM

Immunoblot analysis of pancreatic total homogenate (TH) and zymogen granule membrane (ZGM) fractions using a Gi3-specific antibody after resolution by

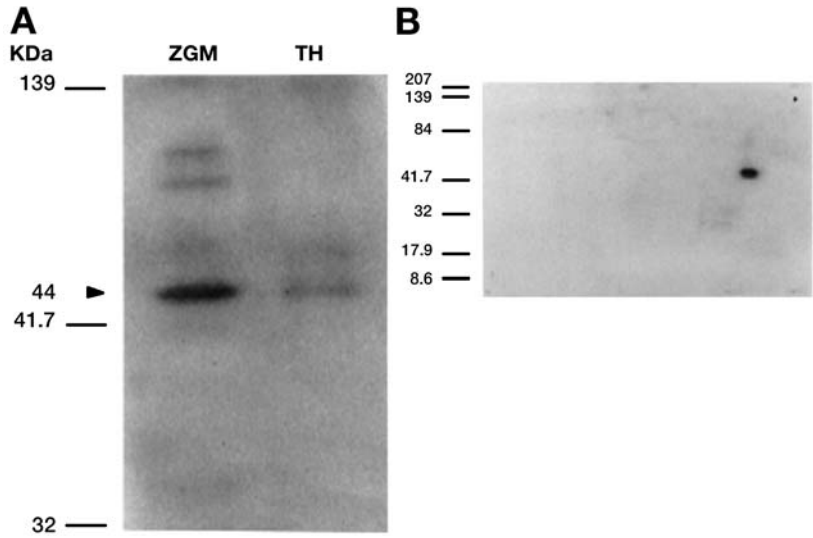

Fig. 2. Immunolocalization and biochemical detection of a $G_{\alpha i3}$ protein with ZGs from rat exocrine pancreas. **(A,B)** Immunoblot analysis. Identification of $G_{\alpha i3}$-immunoreactive antigen associated with ZGM. **(A)** Ten micrograms each of TH and ZGM was resolved using a single-dimension 12.5% SDS gel electrophoresis before electrotransfer onto nitrocellulose and immunoblotting. A 44-kDa immunoreactive band was detected in both fractions but enriched in the ZGM. **(B)** Twenty-five micrograms of ZGM protein was resolved on two-dimensional 16-BAC gel electrophoresis before electrotransfer and immunoblotting using the Gi3-specific antibody. Note a single spot at approx 44 kDa, suggesting that only one Gi3 isoform is present in the ZGM. (From **ref. *17***.)

SDS/PAGE and electrotransfer to nitrocellulose membrane demonstrated a 44-kDa major immunoreactive band in both fractions. An increase in band intensity was found in the ZGM fraction over TH (*see* **Fig. 2A**). An affinity-purified rabbit polyclonal antibody (Santa Cruz Biotechnology) raised against a peptide corresponding to amino acid 345–354 mapping at the carboxy terminus of Gi3 of rat origin was used in the study. No immunoreactive bands were detected in the ZGM fraction when the nitrocellulose with resolved proteins was immunoblotted with affinity-purified Gs-, Gz-, and Gt-specific antibodies (not shown). To determine if more than one Gi isoform was present in ZGM, two-dimensional 16-BAC gel followed by immunoblotting using the Gi3- specific antibody was performed. Results from this study demonstrate a single spot at approximately the 44-kDa mark to be present in ZGM (*see* **Fig. 2B**). The 44-kDa immunoreactive band (single-dimension protein resolution) or spot (two-dimensional protein resolution) was absent in blots that were immunostained with peptide-neutralized antibody (not shown).

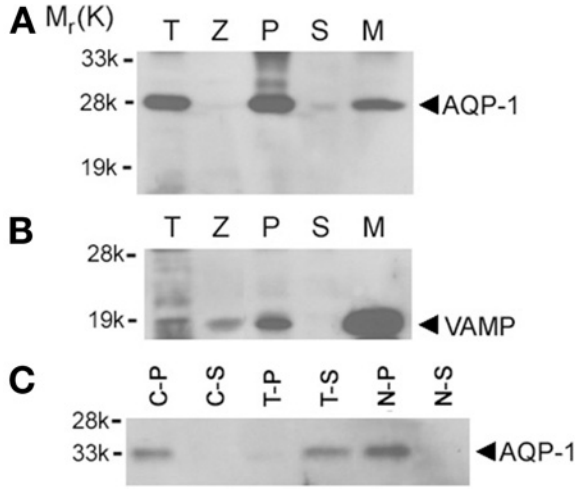

Fig. 3. Twenty micrograms of protein from each of the rat pancreatic fractions, total homogenate (T), zymogen granule (Z), 200,000*g* particulate (P) and supernatant (S) from total homogenates, and zymogen granule membrane (M), were resolved using 12.5% SDS-PAGE. The resolved proteins in each fraction were electrotransferred to nitrocellulose membrane and immunoblotted using AQP1 and VAMP-specific antibodies. The 28-kDa AQP1 immunoreactivity is associated with the M fraction **(A)**. The purity of isolated Z is demonstrated by the enriched presence of VAMP in the M fraction **(B)**. Zymogen granules are membrane-bound secretory vesicles packed with secretory proteins. The membrane fraction constitutes <1% of total granular proteins. Thus, very little AQP1 and VAMP immunoreactivity is detected in total granules, compared with several-fold enrichment in the granule membrane fraction. Affinity of AQP1 association with M was further examined by exposing 10 µg of granule membrane protein to buffer, salt, and detergent **(C)**. After treatment of the granule membrane, the particulate and supernatant fractions were separated by centrifugation at 200,000*g*. Examination of particulate (C-P) and supernatant (C-S) fractions prepared following PBS treatment, treatment with 1% Triton X-100 in PBS (T-P, T-S), or with 1 *M* KCl (N-P, N-S) demonstrates specific and tight association of AQP1 immunoreactivity with M. Exposure of the M to PBS or 1 *M* KCl failed to dislodge the AQP1 immunoreactivity; however, the nonionic detergent Triton X-100 was able to dissociate AQP1 from the granule membrane. (From **ref. *27***.)

3.3. Water Channel AQP1 at ZG Membrane

Pancreatic subcellular fractions ***(2,17,28,30)*** demonstrate the presence of AQP1 immunoreactivity in ZG membrane preparations (*see* **Fig. 3A**). A strong immunoreactive signal was also observed in the pancreatic particulate fraction. Because it is possible for ZG to have been contaminated with other subcellular components enriched in AQP1, it was necessary to determine the purity of the

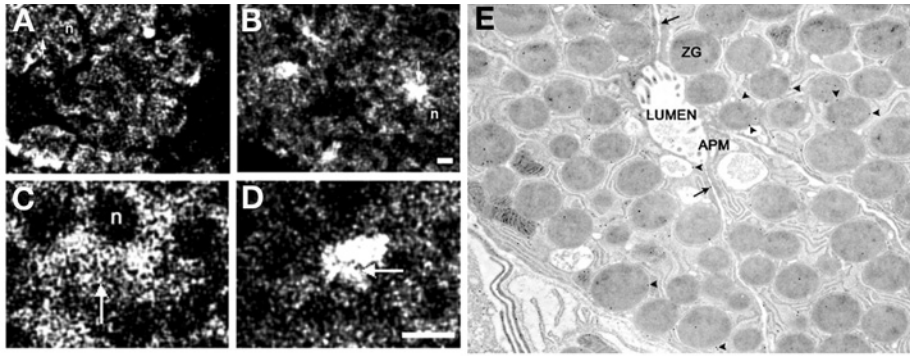

Fig. 4. AQP1 immunofluorescent confocal microscopy on stimulated and resting pancreatic lobules (**A–D**). Pancreatic lobules incubated for 1 h at 37°C in the absence (resting) or presence (stimulated) of the secretagogue carbamylcholine (1×10^{-5} *M*). A fourfold increase in amylase secretion from stimulated pancreatic lobules over resting was observed (data not shown). Following incubation, the lobules were fixed, cryosectioned, and processed for immunofluorescent confocal microscopy. Confocal images of AQP1 immunostained pancreatic tissue in resting **(A,C)** and stimulated **(B,D)** states indicate association of AQP1 with zymogen granules and its possible involvement in secretion. In resting acinar cells, AQP1 appears distributed throughout the cell including the apical region (arrow). The nucleus (n) located at the basolateral end of pancreatic acinar cells is devoid of AQP1-specific immunostaining. Following stimulation of secretion, much of the AQP1 immunoreactivity is localized at the apical region of pancreatic acinar cells where secretion is known to occur. (Bar = 10 μ*M*.) Immunogold electron microscopic (10-nm particles) localization of AQP1 to ZG (arrowheads) **(E)**. Note some AQP1 associated with the cell plasma membrane (arrow). Magnification: ×57,000 (reduced from original magnification). (From **ref. *27***.)

ZG preparation. The purity of ZG and the ZG membrane fractions were further determined by the enriched presence of VAMP immunoreactivity (*see* **Fig. 3B**). VAMP, also known as synaptobrevin, is a vesicle-associated membrane protein present in ZG membranes. A significant enrichment of VAMP immunoreactivity was observed in ZG membrane, compared to other pancreatic fractions. To determine the type of association of AQP1 with ZGs, the ZG membrane was treated with salt (1 *M* KCl) and a nonionic detergent (1% Triton X-100). Detergent treatment released the AQP1 immunoreactivity from ZG membranes, but salt had no effect (*see* **Fig. 3C**). These results show that AQP1, as its structure suggests ***(36,37)***, is tightly associated with the ZG membrane. To further determine the distribution of AQP1 in pancreatic acinar cells, AQP1 immunoreactivity was examined ***(38)***, using both light (*see* **Fig. 4A–D**) and electron microscopy (*see* **Fig. 4E**). Pancreatic acinar cells are polarized secretory cells which contain apically located ZGs. Abundant AQP1 immunoreactivity was

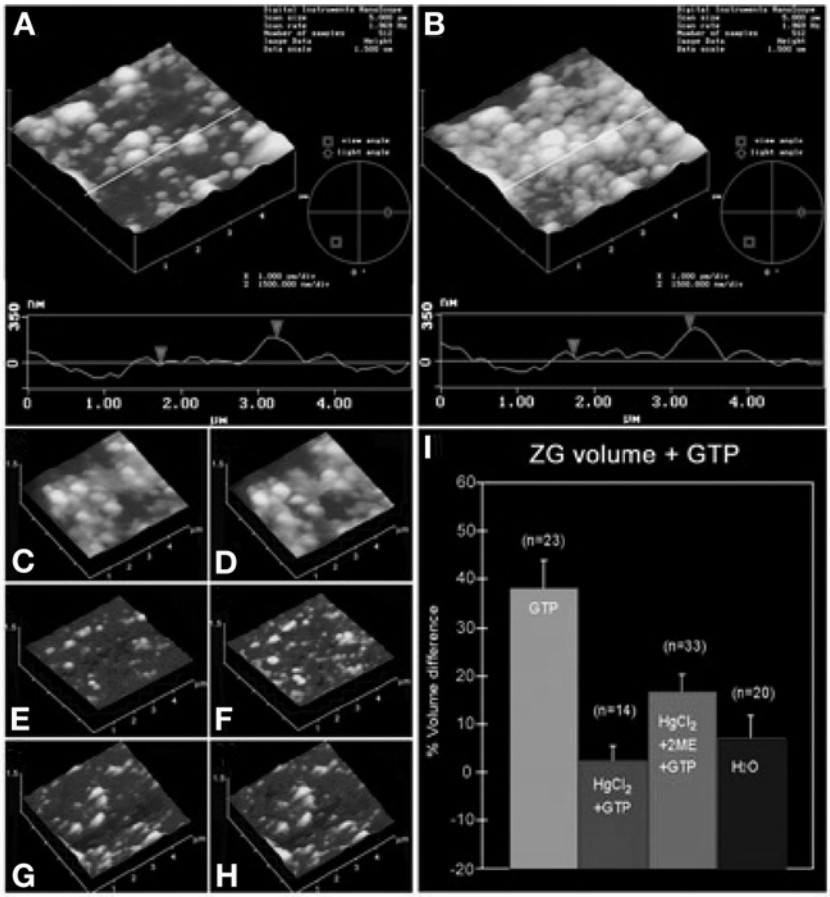

Fig. 5. Three-dimensional AFM images and section analysis of ZG, untreated **(A,B)** or pretreated with 25 μ*M* HgCl2 **(C,D)** and pretreated with 25 μ*M* $HgCl_2$ followed by 100 μ*M* β-mercaptoethanol **(E,F)** before **(A,C,E)** and after **(B,D,F)** exposure to 40 μ*M* GTP. Notice the increase in size of ZG (from A to B and I) in the three-dimensional array, section analysis, and bar graph, following exposure to GTP. Pretreatment of ZG with $HgCl_2$ abolishes the GTP effect (from C to D and I). However, the inhibitory effect of $HgCl_2$ is partially reversed in the presence of β-mercaptoethanol (from E to F and I). Incubation of ZG in water instead of 125 m*M* KCl–Mes buffer, pH 6.5, has little effect on ZG size (time 0 min G to time 30 min H and I). (From **ref. *27*.**)

detected at the apical region of these cells. In resting acini (*see* **Fig. 4A–D**), AQP1 immunoreactivity was detectable throughout the cell, but its primary localization was at the apical region. Electron microscopy further confirms the presence of AQP1 at the ZG membrane (*see* **Fig. 4E**). It is well established that following a secretory stimulus, there is release of granular contents at the

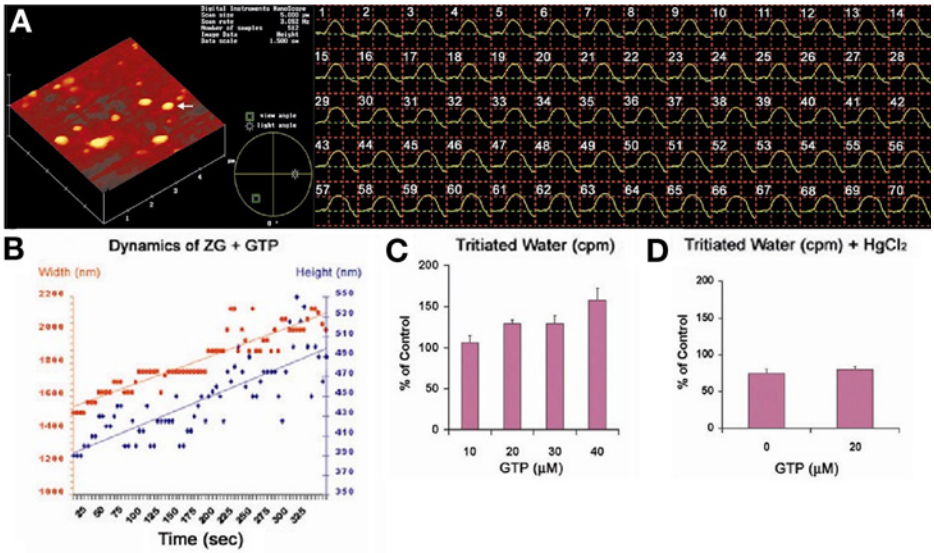

Fig. 6. The height and width of a single ZG (arrow) is monitored in seconds, following exposure to 40 μ*M* GTP **(A,B)**. Notice the linear time-dependent increase in both height and width of the ZG following exposure to GTP A GTP dose-dependent increase in tritiated water entry is observed in ZG **(C)**. Exposure of ZG to $HgCl_2$ inhibits both basal and GTP-induced tritiated water entry into ZG **(D)**. (*See* Color Plate 18 following p. 274. From **ref.** *27*.)

apical lumen of pancreatic acini. Immunocytochemistry performed using light microscopy demonstrated intense AQP1-specific labeling at the apical region of the cell (*see* **Fig. 4B,D**), suggesting the involvement of AQP1 in secretion.

3.4. GTP-Induced ZG Swelling Is $HgCl_2$ Sensitive

As previously demonstrated, exposure to GTP results in swelling (percent volume increase = 38.22 ± 5.87; mean ± S.E.) of isolated ZG preparations (*see* **Figs. 5A,B,I** and **6A–C**). Within seconds, following exposure to 40 μ*M* GTP, a marked increase in water entry into ZG was demonstrated (*see* **Fig. 6A,B**). Water permeability of ZG was GTP dose dependent, as assayed by using the entry of tritiated water (*see* **Fig. 6C**). The increased entry of tritiated water was 6.5% over control in the presence of 10 μ*M* GTP, 29.6% in the presence of 20 μ*M* GTP, and 58% in the presence of 40 μ*M* GTP. However, exposure of ZG to $HgCl_2$, a known inhibitor of AQP1 ***(18,39)***, results in inhibition of both the basal (75.1 ± 6.17% of control) as well as the GTP-mediated (80.43 ± 3.55% of control) water permeability (*see* **Figs. 5C,D,I** and **6D**). The effect of $HgCl_2$ on ZG was reversed in the presence of 1 m*M* β-mercaptoethanol (*see* **Fig. 5E,F,I**), as

demonstrated by a 16.83 ± 3.53% GTP-induced increase in volume of $HgCl_2$-treated vesicles following exposure to 1 m*M* β-mercaptoethanol.

3.5. Functional AQP1 at ZG Membrane

To determine if the GTP-induced water entry was the result of the AQP1 water channel function or osmosis driven, isolated ZGs were incubated in water and their size was monitored. Isolated ZG incubated in water had little effect (*see* **Fig. 5G,H,I**), as shown by no significant change in percent ZG volume over control (7.32 ± 4.51%). The presence of functional AQP1 in ZG membranes was confirmed from tritiated water (^3H_2O) permeability experiments on isolated ZG. ZGs were incubated in buffer containing ^3H_2O, in the presence and absence of GTP and/or $HgCl_2$. GTP is known to induce swelling of isolated ZGs ***(17)***. Exposure of isolated ZGs to GTP (10–40 μ*M*) results in an increase in water entry in a dose-dependent manner (*see* **Fig. 6C**). In the presence of $HgCl_2$, GTP-induced water entry was inhibited (*see* **Fig. 6D**). Isolated ZGs are stable for hours in low-pH (pH 6–6.5) buffers. At neutral or alkaline pH, isolated ZGs rapidly lyse. All studies were therefore performed in pH 6.5 buffer. These results, however, do not exclude the possibility that yet unidentified mercury-sensitive water channels might contribute to GTP-stimulable water entry into ZGs. This issue was addressed by introducing, into ZGs, AQP1-specific antibody raised against the carboxyl domain of the water channel.

3.6. AQP1 Regulates ZG Swelling

The introduction of AQP1-specific antibody into isolated ZG was carried out by permeabilizing ZG using SLO. We next carried out experiments to determine whether the AQP1 antibody actually entered the SLO-treated ZGs and, if so to determine their distribution within the ZG. Both Western blot assay and immuno-electron microscopy demonstrate the entry of AQP1 antibody into ZGs (*see* **Fig. 7A–E**; *see* Color Plate 19 following p. 274). When intact and permeabilized ZGs were separately exposed to the AQP1 antibody, resolved using SDS-PAGE, followed by transfer to nitrocellular membrane and immunoblot probed using a secondary antibody conjugated to a chemiluminescent marker, the AQP antibody was detected in the SLO-treated ZG, demonstrating entry of the antibody. No detectable signal was seen in the intact ZG fraction exposed to the AQP1 antibody (*see* **Fig. 7A**). Electron microscopy performed in the intact and SLO-treated ZG demonstrated intense immunogold localization in the SLO-treated ZGs, confirming AQP1 entry into the ZGs. Specific immunogold labeling at the luminal side of the ZG membrane in the SLO-treated batch further confirms binding of the antibody to the carboxy domain of AQP1. When AQP1-specific antibody was introduced into SLO permeabilized ZGs (*see* **Fig. 7A–F**),

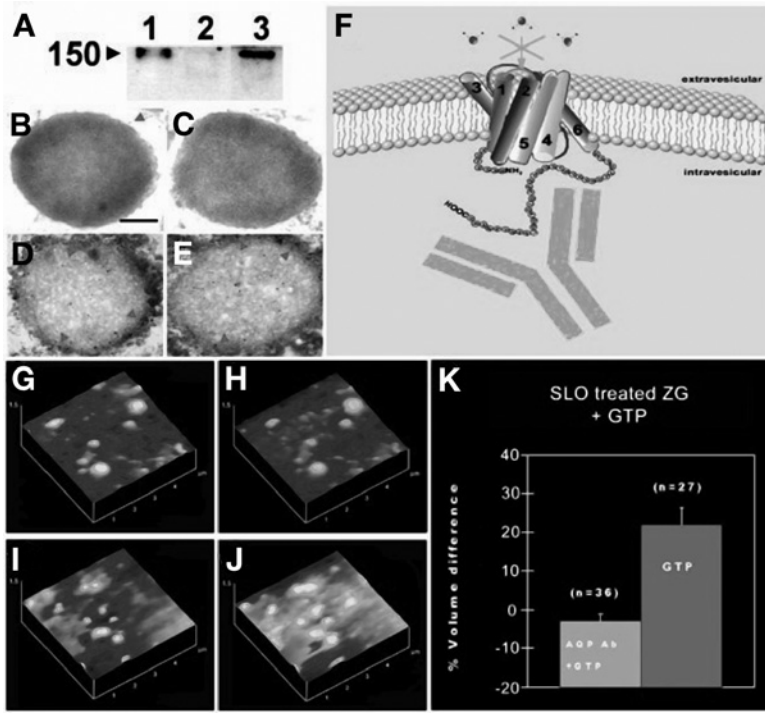

Fig. 7. Immunoblot assay demonstrating the presence of AQP1 antibody in SLO permeabilized ZG **(A)**. Lane 1 is AQP1 antibody alone; lane 2 is nonpermeable ZG exposed to antibody; lane 3 is permeable ZG exposed to AQP1 antibody. Immuno-electron micrographs of intact ZGs exposed to AQP1 antibody demonstrate little labeling **(B,C)**. (Bar = 200 nm.) Contrarily, SLO-treated ZG demonstrate intense gold labeling at the luminal side of the ZG membrane **(D,E)**. AQP1 regulates GTP-induced water entry in ZG. Schematic diagram of ZG membrane depicting AQP1-specific antibody binding to the carboxy domain of AQP1 at the intragranular side, to block water gating **(F)**. AQP1 antibody introduced into ZG blocks GTP-induced water entry and swelling (from **G** to **H,** following GTP exposure; **G,H,K**). However, only vehicle introduced into ZG, retains the GTP-stimulable effect (from **I** to **J**, following GTP exposure; **I–K**). (*See* Color Plate 19 following p. 274. From **ref.** ***27***.)

GTP-induced water entry was inhibited (**Fig. 7G,H,K**). However, in the absence of AQP1-specific antibody, SLO permeabilized ZGs elicit strong GTP-induced swelling (% volume increase of 21.95 ± 4.42; *see* **Fig. 7I–K**). These studies demonstrate that at pH 6.5, AQP1 participates in GTP-induced gating of water in ZG of pancreatic acinar cells. Previous studies demonstrated that the carboxyl domain of AQP1 does not participate in water entry ***(40)***. However, the inhibition of AQP1 by the antibody could result from the structural distortion of AQP1 by binding of the comparatively larger antibody molecule. To understand

the detailed pathway of GTP-induced signaling in the regulation of AQP1 in ZG membrane, further studies are being conducted. Studies using liposomes reconstituted with AQP1, the $G_{\alpha i3}$ protein, and other signaling molecules will help elucidate the molecular mechanism of $G_{\alpha i3}$-mediated and GTP-induced AQP1-involvement in water entry into ZG.

Acknowledgments

This work was supported in part by research grants DK56212 and NS39918 to B.P.J. from the National Institutes of Health. S.J.C. is a recipient of an NIH postdoctoral fellowship award (DK60368).

References

1. Alvarez de Toledo, G., Fernandez-Chacon, R., and Fernandez, J. M. (1993) Release of secretory products during transient vesicle fusion. *Nature* **363,** 554–558.
2. Curran, M. J. and Brodwick, M. S. (1991) Ionic control of the size of the vesicle matrix of beige mouse mast cells. *J. Gen. Physiol.* **98,** 771–790.
3. Monck, J. R., Oberhauser, A. F., Alvarez de Toledo, G., and Fernandez, J. M. (1991) Is swelling of the secretory granule matrix the force that dilates the exocytotic fusion pore? *Biophys. J.* **59,** 39–47.
4. Finkelstein, A., Zimmerberg, J., and Cohen, F. S. (1986) Osmotic swelling of vesicles: its role in the fusion of vesicles with planar phospholipid bilayer membranes and its possible role in exocytosis. *Annu. Rev. Physiol.* **48,** 163–174.
5. Fernandez, J. M., Villalon, M., and Verdugo, P. (1991) Reversible condensation of mast cell secretory products in vitro. *Biophys. J.* **59,** 1022–1027.
6. Holz, R. W. (1986) The role of osmotic forces in exocytosis from adrenal chromaffin cells. *Annu. Rev. Physiol.* **48,** 175–189.
7. Almers, W. (1990) Exocytosis. *Annu. Rev. Physiol.* **52,** 607–624.
8. Gasser, K. W., DiDomenico, J., and Hopfer, U. (1988) Secretagogues activate chloride transport pathways in pancreatic zymogen granules. *Am. J. Physiol.* **254,** G93–G99.
9. Fuller, C. M., Deetjen, H. H., Piiper, A., and Schulz, I. (1989) Secretagogue and second messenger-activated Cl^- permeabilities in isolated pancreatic zymogen granules. *Pflugers Arch.* **415,** 29–36.
10. Fuller, C. M., Eckhardt, L., and Schulz, I. (1989) Ionic and osmotic dependence of secretion from permeabilised acini of the rat pancreas. *Pflugers Arch.* **413,** 385–394.
11. Gasser, K. W. and Hopfer, U. (1990) Chloride transport across the membrane of parotid secretory granules. *Am. J. Physiol.* **259,** 413–420.
12. Thevenod, F., Gasser, K. W., and Hopfer, U. (1990) Dual modulation of chloride conductance by nucleotides in pancreatic and parotid zymogen granules. *Biochem. J.* **272,** 119–126.
13. Piiper, A., Plusczyk, T., Eckhardt, L., and Schulz, I. (1991) Effects of cholecystokinin, cholecystokinin JMV-180 and GTP analogs on enzyme secretion from

permeabilized acini and chloride conductance in isolated zymogen granules of the rat pancreas. *Eur. J. Biochem.* **197,** 391–398.
14. Thevenod, F., Chathadi, K. V., and Hopfer, U. (1992) ATP-sensitive K^+ conductance in pancreatic zymogen granules: block by glyburide and activation by diazoxide. *J. Membr. Biol.* **129,** 253–266.
15. Takuma, T., Ichida, T., Okumura, K., Sasaki, Y., and Kanazawa, M. (1993) Effects of valinomycin on osmotic lysis of zymogen granules and amylase exocytosis from parotid acini. *Am. J. Physiol.* **264,** G895-G901.
16. Thevenod, F., Hildebrandt, J-P., Striessnig, J., de Jong, H. R., and Schulz, I. (1996) Chloride and potassium conductances of mouse pancreatic zymogen granules are inversely regulated by a approximately 80-kDa mdr1a gene product. *J. Biol. Chem.* **271,** 3300–3305.
17. Jena, B. P., Schneider, S. W., Geibel, J. P., Webster, P., Oberleithner, H., and Sritharan, K. C. (1997) Gi regulation of secretory vesicle swelling examined by atomic force microscopy. *Proc. Natl. Acad. Sci. USA* **94,** 13,317–13,322.
18. Preston, G. M., Carroll, T. P., Guggino, W. B., and Agre, P. (1992) Appearance of water channels in *Xenopus* oocytes expressing red cell CHIP28 protein. *Science* **256,** 385–387.
19. Ito, H., Tung, R. T., Sugimoto, T., et al. (1992) On the mechanism of G protein beta gamma subunit activation of the muscarinic K+ channel in guinea pig atrial cell membrane. Comparison with the ATP-sensitive K+ channel. *J. Gen. Physiol.* **99,** 961–983.
20. Schwiebert, E. M., Kizer, N., Gruenert, D. C., and Stanton, B. A. (1992) GTP-binding proteins inhibit cAMP activation of chloride channels in cystic fibrosis airway epithelial cells. *Proc. Natl. Acad. Sci. USA* **89,** 10,623–10,627.
21. Kirsch, G. E., Codina, J., Birnbaumer, L., and Brown, A. M. (1990) Coupling of ATP-sensitive K^+ channels to A1 receptors by G proteins in rat ventricular myocytes. *J. Am. J. Physiol.* **259,** H820–H826.
22. Schwiebert, E. M., Light, D. B., Fejes-Toth, G., Naray-Fejes-Toth, A., and Stanton, B. A. (1990) A GTP-binding protein activates chloride channels in a renal epithelium. *J. Biol. Chem.* **265,** 7725–7728.
23. Marinelli, R. A., Pham, L., Agre, P., and LaRusso, N. F. (1997) Secretin promotes osmotic water transport in rat cholangiocytes by increasing aquaporin-1 water channels in plasma membrane. Evidence for a secretin-induced vesicular translocation of aquaporin-1. *J. Biol. Chem.* **272,** 12,984–12,988.
24. Knepper, M. A. (1994) The aquaporin family of molecular water channels. *Proc. Natl. Acad. Sci. USA* **91,** 6255–6258.
25. Yasui, M., Hazama, A., Kwon, T. H., Nielsen, S., Guggino, W. B., and Agre, P. (1999) Rapid gating and anion permeability of an intracellular aquaporin**.** *Nature* **402,** 184–187.
26. Knepper, M. A. and Inoue, T. (1997) Regulation of aquaporin-2 water channel trafficking by vasopressin. *Curr. Opin. Cell Biol.* **9,** 560–564.
27. Cho, S. J., Abdus Sattar, A. K., Jeong, E. H., et al. (2002) Aquaporin 1 regulates GTP-induced rapid gating of water in secretory vesicles. *Proc. Natl. Acad. Sci. USA* **99,** 4720–4724.

28. Jena, B. P., Padfield, P. J., Ingebritsen, T. S., and Jamieson, J. D. (1991) Protein tyrosine phosphatase stimulates Ca(2+)-dependent amylase secretion from pancreatic acini. *J. Biol. Chem.* **266,** 17,744–17,746.
29. Cameron, R. S., Cameron, P. L., and Castle, J. D. (1986) A common spectrum of polypeptides occurs in secretion granule membranes of different exocrine glands. *J. Cell Biol.* **103,** 1299–1313.
30. Rosenzweig, S. A., Miller, L. J., and Jamieson, J. D. (1983) Identification and localization of cholecystokinin-binding sites on rat pancreatic plasma membranes and acinar cells: a biochemical and autoradiographic study. *J. Cell Biol.* **96,** 1288–1297.
31. Bradford, M. M. (1976) A rapid and sensitive method for the quantitation of microgram quantities of protein utilizing the principle of protein-dye binding. *Anal. Biochem.* **72,** 248–254.
32. Laemmli, U. K. (1970) Cleavage of structural proteins during the assembly of the head of bacteriophage. T4. *Nature* **227,** 680–685.
33. Bendayan, M. (1984) Protein A-gold immunocytochemistry: technical approach, applications and limitations. *J. Electron Microsc. Tech.* **1,** 243–270.
34. Schneider, S. W., Sritharan, K. C., Geibel, J. P., Oberleithner, H., and Jena, B. P. (1997) Surface dynamics in living acinar cells imaged by atomic force microscopy: identification of plasma membrane structures involved in exocytosis. *Proc. Natl. Acad. Sci. USA* **94,** 316–321.
35. Henderson, R. M., Schneider, S., Li, Q., Hornby, D., White, S. J., and Oberleithner, H. (1996) Imaging ROMK1 inwardly rectifying ATP-sensitive K^+ channel protein using atomic force microscopy. *Proc. Natl. Acad. Sci. USA* **93,** 8756–8760.
36. Walz, T., Hirai, T., Murata, K., et al. (1997) The three-dimensional structure of aquaporin-1. *Nature* **387,** 624–627.
37. Cheng, A., van Hoek, A. N., Yeager, M., Verkman, A. S., and Mitra, A. K. (1997) Three-dimensional organization of a human water channel. *Nature* **387,** 627–630.
38. Jena, B. P., Gumkowski, F. D., Konieczko, E. M., von Mollard, G. F., Jahn, R., and Jamieson, J. D. (1994) Redistribution of a rab3-like GTP-binding protein from secretory granules to the Golgi complex in pancreatic acinar cells during regulated exocytosis. *J. Cell Biol.* **124,** 43–53.
39. Agre, P., Bonhivers, M., and Borgnia, M. J. (1998) The aquaporins, blueprints for cellular plumbing systems. *J. Biol. Chem.* **273,** 14,659–14,662.
40. Murata, K., Mitsuoka, K., Hirai, T., et al. (2000) Structural determinants of water permeation through aquaporin-1. *Nature* **407,** 599–605.